

Direct force measurements for testing the *LISA Pathfinder* gravitational reference sensor

A Cavalleri¹, G Ciani², R Dolesi², M Hueller², D Nicolodi², D Tombolato²,
P J Wass², W J Weber², S Vitale² and L Carbone^{2,3}

¹ Centro Fisica degli Stati Aggregati, 38050 Povo (TN), Italy

² Dipartimento di Fisica, Università di Trento, and INFN Gruppo collegato di Trento,
via Sommarive 14, 38050 Povo (TN), Italy

E-mail: wass@science.unitn.it

Received 31 October 2008, in final form 20 January 2009

Published 20 April 2009

Online at stacks.iop.org/CQG/26/094012

Abstract

We present results of testing of the *LISA Pathfinder* gravitational reference sensor (GRS) using a 4-test-mass torsion pendulum facility aimed at measuring low-frequency force-noise sources in the *LISA* and *LISA Pathfinder* frequency band. This pendulum, for the first time, allows us to make measurements which are sensitive to all forces acting along the sensitive axis of the test mass, not only those that create a torque. We will report on a campaign of testing using the *LISA Pathfinder* ‘engineering model’ prototype GRS which has set upper limits on the overall force noise acting on the test mass contributed by surface effects within the sensor at a level of $100 \text{ fN Hz}^{-1/2}$ at 2 mHz and measured specific sources of unwanted disturbances. These sources include forces arising from the electrostatic coupling between the sensor and test-mass motion, electrostatic fields due to surface-potential variations and thermal-gradient effects within the sensor. Finally, we describe the extension of this campaign to the *LISA Pathfinder* flight-model replica GRS which will be crucial in verifying the design and performance of the flight instrument.

PACS numbers: 04.80.Nn, 07.87.+v, 95.55.Yn

(Some figures in this article are in colour only in the electronic version)

1. Introduction

LISA is a joint ESA/NASA project to observe gravitational waves in space originating from a range of galactic, extra-galactic and cosmological sources [1]. The measurement will be

³ Current address: School of Physics and Astronomy, University of Birmingham, Edgbaston, Birmingham B15 2TT, UK.

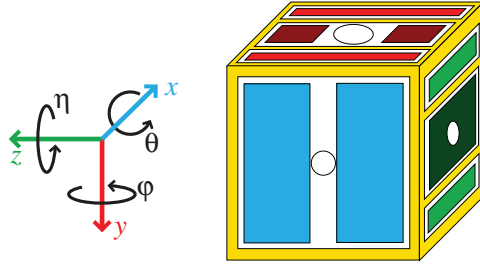


Figure 1. A schematic of the *LISA Pathfinder* gravitational reference sensor, there are two sensing electrodes on each face, two injection electrodes on the y-faces and one on the z-faces (shaded darker).

achieved by detecting the relative movement of free-flying test particles in a constellation of three spacecraft separated by 5 million km. These particles are 2 kg gold–platinum test masses, each shielded from external disturbances by a spacecraft. The spacecraft use a combination of sensitive test-mass position detection and micro-Newton thrusters to follow the geodesic motion of the test mass in one degree of freedom. In other degrees of freedom, the test mass is actuated to follow the motion of the spacecraft. The position measurement in the sensitive degree of freedom is carried out with a heterodyne interferometer, the sensing and actuation in other degrees of freedom is achieved with a capacitive gravitational reference sensor.

The level of free-fall required for *LISA* sets a limit on the parasitic acceleration on the test mass of $3 \times 10^{-15} \text{ m s}^{-2} \text{ Hz}^{-1/2}$ at 0.1 mHz, the ambitious nature of this goal has motivated a dedicated mission, *LISA Pathfinder*, aimed at demonstrating the technology required to reach a level of free-fall within one order of magnitude of the *LISA* performance in acceleration noise and frequency, $3 \times 10^{-14} \text{ m s}^{-2} \text{ Hz}^{-1/2}$ at 1 mHz [2].

Free-fall is limited by stray forces acting directly on the test mass, and the coupling of force gradients with movement of the spacecraft relative to the test mass because of noisy external forces. The gravitational reference sensor (GRS), being separated from the test mass by only some millimetres, is an important source of noisy forces and force gradients.

The GRS, illustrated in figure 1, is a capacitive position sensor, using a combination of 6 ‘injection’ electrodes to apply a 100 kHz AC bias to the test mass and a further 12 sensing electrodes for position sensing and force actuation in 6 degrees of freedom [3].

1.1. Principal disturbances

Unwanted forces acting on the test mass may arise from thermal gradients in the sensor, electrostatic, magnetic and gravitational forces acting on the test mass, cross-talk of actuation-force noise in other degrees of freedom into the sensitive axis and thermal dissipation effects in the sensor. The most important source of force gradients at the test mass originate from the gravitational field of the spacecraft, electrostatic actuation forces and AC sensing bias voltages.

Disturbances on the test mass can be separated into those that can be attributed to the sensor and those that come from the spacecraft. Forces acting on the spacecraft directly such as thruster noise and solar radiation pressure and force gradients caused by the spacecraft self-gravity can only be tested in the space environment. The remainder of the forces and force gradients, originate from the sensor. In principle, therefore, the technology risk of the mission can be significantly reduced by testing the GRS on ground. In practice, however, achieving low-frequency force sensitivity in the sub-pico Newton regime in a 1-g environment

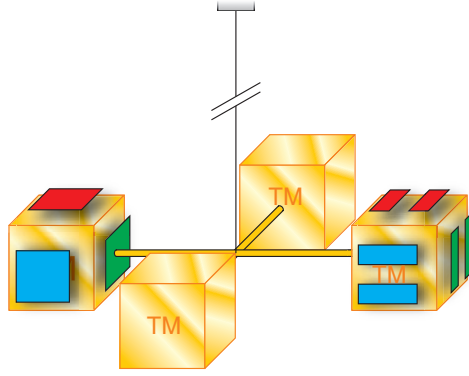


Figure 2. A schematic of the 4-test-mass torsion pendulum. The layout of the sensing electrodes of the GRS is shown, with two sensing electrodes on each face. On the opposing test mass is the simplified custom-built sensor with one sensing electrode on each x and z face and one injection electrode on each y face.

is extremely difficult. Such measurements have been demonstrated in previous work using a 1-mass torsion pendulum and capacitive sensors similar to the design envisaged for *LISA* and *LISA Pathfinder* [4, 5] measuring the torque in the ϕ direction, about the suspension axis. This has allowed stringent limits to be set on the force noise arising from the sensor [6, 7] and measurements of several individual noise sources such as those arising from thermal gradients [8], variations of stray voltages [9], random charging effects [10] and the coupling of test-mass motion with force gradients in the sensor [5].

One can imagine, however, forces or combinations of forces arising from the sensor that could jeopardize the goals of *LISA* or *LISA Pathfinder* which would not create a torque on the test mass. Calculations of total force arising from the sensor and measurements of specific forces are dependent on a model describing the arm length with which those forces act on the test mass. A more reassuring experimental set-up would be one which is sensitive to all forces along the translational axis of the test mass as is the case in *LISA* and *LISA Pathfinder*.

1.2. 4-test-mass pendulum

The 4-test-mass torsion pendulum, illustrated in figure 2, was developed to make direct measurements of forces acting on a test mass along the translational degree of freedom [11]. Instead of suspending a single test, four test masses are mounted on a cross-shaped structure suspended from its centre by a $50\ \mu\text{m}$ tungsten fibre similar to those used previously in the 1-mass torsion pendulum. The shape of the inertial member was chosen to minimize the quadrupole moment which can couple with gravity gradients to cause a noisy torque [12].

The total mass of the pendulum, $0.46\ \text{kg}$, is approximately four times that of the 1-mass pendulum, necessitating a torsional fibre with twice the diameter. The thermal torque noise of such a fibre is given by $4k_{\text{B}}T\frac{\Gamma}{\omega Q}$ and since $\Gamma \propto d^4$, the thermal torque noise is increased by a factor 16 in power (a factor 4 in the spectral density). However, forces on the test mass create a torque through the arm length ($0.105\ 65\ \text{m}$) which is ~ 10 times larger than that estimated for the 1-mass pendulum. The overall force sensitivity of the 4-mass pendulum is therefore better by a factor ~ 2 .

Two opposite test masses are surrounded by capacitive sensors, one the GRS, the other, a custom-built, simplified sensor which can be used to balance the electrostatic force gradient introduced by the GRS by producing the same gradient on the opposite test mass and to provide

a differential readout of the pendulum angle. It is similar in design to the GRS but has larger gaps (8 mm instead of 4 mm) between the test mass and electrodes. This renders the unwanted surface force disturbances acting on the second test mass significantly smaller than those produced by the GRS. The sensor has 1 electrode per face, and so measures position in x and z only, while using the y electrodes to apply the sensing bias. The differential measurement from two capacitive sensors is calibrated against a 2 degree of freedom optical autocollimator incident on a mirror fixed to the pendulum torsional member. The autocollimator provides an independent angular readout of comparable precision to the capacitive sensors.

The GRS is mounted on a motor sled which allows its position in the x -axis to be controlled precisely. A system of heaters also connected to the GRS allows heating of the x -faces, while thermometers monitor the temperature of several points on the capacitive sensors, and the vacuum chamber. An ion gauge provides a measure of the pressure in the experimental apparatus, which is kept thermalized by an air-conditioned, insulating chamber.

In this paper we report on a series of measurements conducted using the *LISA Pathfinder* engineering model (EM) prototype GRS, in preparation for a testing campaign using a flight-model replica GRS. We describe measurements of forces arising from thermal gradients in the sensor, the total stiffness attributable to the sensor coming from AC biasing voltages and other force gradients at the test mass, and of stray voltages on the sensor surfaces.

2. Sensor noise

The autocollimator and capacitive sensors give independent measures of the pendulum angle which is converted to a torque through the equation of motion while the overall excess noise is calculated from the cross-spectrum of the force noise calculated from the two independent readouts. This procedure is the same as that used in previous torsion-pendulum measurements [7]. In the case of the 4-test-mass pendulum, however, we can be sure that all forces acting along the x -axis are creating a torque and that the arm length at which they act is well known.

Figure 3(a) shows the averaged noise spectra measured by the autocollimator and the combination of capacitive sensors in 12 measurement ‘runs’ made over the course of 9 months. Also shown is the thermal noise of the suspension fibre. Both the autocollimator and capacitive readout showed force sensitivity within a factor 2–3 of the thermal limit around 1 mHz, with the capacitive readout being better above 1 mHz and below 0.5 mHz.

An upper limit of the noise acting on the test mass which originates from the sensor is given by the cross-correlation of the two measurements with the thermal noise of the fibre subtracted. This curve, shown in figure 3(b) shows a minimum of $10^{-13} \text{ N s}^{-2} \text{ Hz}^{-1/2}$ at 2 mHz. At this frequency, the upper limit is close to the total force-noise budget acting on one test mass of *LISA Pathfinder* [13].

3. Thermal gradients

Thermal gradients in the sensor create a force on the test mass in three ways—the radiometer effect, radiation pressure and differential outgassing. These effects have been described in detail and measured using the 1-mass torsion pendulum in a geometry sensitive only to thermal gradient torques [8]. A detailed derivation of the forces arising from each effect can be found in this previous work, here we state the effects in a form relevant to the GRS on the 4-mass pendulum configuration. First, the thermal gradient, ΔT_x , sets up a pressure differential in the residual gas in the sensor at an average pressure P_0 , giving rise to a net force

$$F_x = \alpha_R \frac{AP_0}{4T_0} \Delta T_x, \quad (1)$$

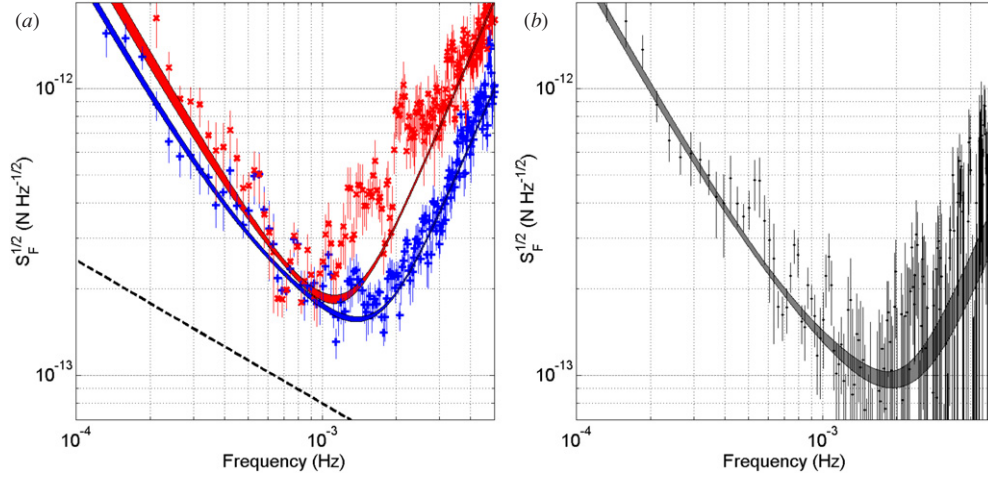


Figure 3. (a) The spectrum of the force on the test mass with fit and associated $1 - \sigma$ errors, measured by the autocollimator (\times and upper curve) and the capacitive sensors ($+$ and lower curve). The dashed line indicates the limiting thermal noise of the pendulum suspension fibre. (b) The cross-spectral density of the force measured by the autocollimator and capacitive sensors with the thermal noise subtracted.

where A is the area of one face of the test mass, T_0 is the average temperature of the sensor and α_R is a factor accounting for gas molecules incident on the y and z faces of the test mass contributing a force along x . The hotter side of the sensor will also emit more energetic photons creating a net force due to radiation pressure

$$F_x = \alpha_{RP} A \frac{8\sigma}{3c} T_0^3 \Delta T_x, \quad (2)$$

where σ is the Stefan–Boltzmann constant, c is the speed of light and α_{RP} is a factor accounting the test-mass reflectivity and radiation with a momentum component along x striking the y and z faces. Finally, thermally activated outgassing of adsorbents on the sensor surfaces will be greater on the hotter side of the GRS, creating a pressure differential across the test mass and a resulting force. This effect depends on the amount and type of adsorbed impurities on the sensor surfaces and since these are unknown it is difficult to model precisely.

The measurement procedure followed is similar to that described in [8], in order to excite a coherent torque on the pendulum in the measurement band, an oscillating temperature gradient is created by applying a low-frequency square-wave voltage to heaters on the $+x$ -face and the same signal, 180-degrees out of phase on the $-x$ heaters. The important difference in using the 4-mass pendulum is that the temperature difference which excites a force is between opposing x -faces of the sensor and not between the two-halves of the same x -face. Using the 1-mass configuration, detailed modelling was required to determine the temperature distribution inside the sensor produced by alternately heating one half of the sensor face and then the other. Uniformly heating a whole sensor face, the relation between the measured temperature on the outside of the sensor and that inside is much simpler.

The force acting on the test mass as a function of the temperature gradient across the sensor is shown in figure 4(a). As expected, the force is linear in the temperature gradient. For this measurement, the average sensor temperature was 309.4 ± 0.1 K and the pressure measured in the experiment vacuum chamber was 10^{-5} Pa. The linearity of the force per unit temperature gradient with increasing pressure is well demonstrated by figure 4(b) over the range $1\text{--}20 \times 10^{-5}$ Pa and at an average temperature of 295.2 ± 0.1 and 309.4 ± 0.1 K. The

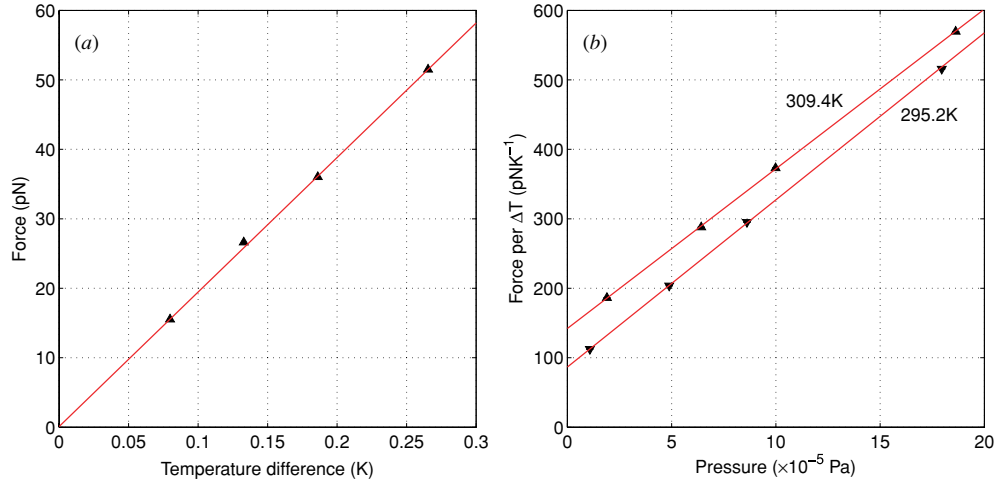


Figure 4. (a) The force measured on the pendulum at the frequency of the temperature modulation plotted against the temperature difference between the sensor x faces. This measurement was made for $T_0 = 309.4$ K and $P_0 \simeq 10^{-5}$ Pa. (b) The force per unit temperature gradient plotted as a function of the measured pressure, here two measurements are shown for $T_0 = 295.2$ K (down triangles) and 309.4 K (up triangles). Errorbars are smaller than the data markers.

slopes calculated from the fits to the data agree with the values predicted by (1) to within 10%, the measured intercepts of the fits are some 10–14 times greater than the expected radiation pressure contribution calculated from (2).

At 295.2 K, extrapolating to the expected pressure in the sensor in space, 10^{-5} Pa, we estimate a force per unit temperature gradient of 100 pN K^{-1} . For *LISA*, the required in-band temperature stability is $10 \text{ } \mu\text{K Hz}^{-1/2}$ while for *LISA Pathfinder* it is relaxed by a factor 10. We therefore expect a thermal-gradient related force of $1 \text{ fN Hz}^{-1/2}$ on-board *LISA*, which is the budgeted value [13]. Given the measured intercepts from figure 4(b), outgassing is an important contribution to this noise, so measuring this value with a ‘dirty’ sensor (one which was not assembled in clean conditions) can give us some confidence in achieving this goal for *LISA*.

4. Stray surface voltages

The electrostatic force acting on the test mass along the x -axis is given by

$$F_x = \frac{1}{2} \sum_i \frac{\partial C_i}{\partial x} (V_i - V_{\text{TM}})^2. \quad (3)$$

The test-mass potential V_{TM} is itself dependent on the voltages on the i sensor surfaces, V_i , each with a capacitance with respect to the test mass of C_i as well as the free charge on the test mass, q ,

$$V_{\text{TM}} = \frac{q}{C_T} + \frac{1}{C_T} \sum_i C_i V_i + \alpha_{\text{inj}} V_{\text{inj}} \sin(\omega_{\text{inj}} t). \quad (4)$$

The final term is the AC sensing bias induced capacitively using a $\omega_{\text{inj}}/2\pi = 100 \text{ kHz}$ sinusoidal voltage with an amplitude of V_{inj} to the injection electrodes. $\alpha_{\text{inj}} = \sum C_{\text{inj}}/C_T$ is the ratio of the total injection capacitance with respect to the test mass to the total test mass capacitance.

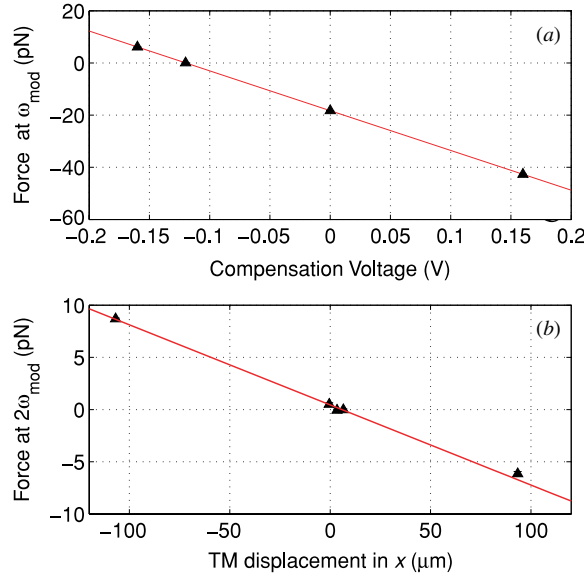


Figure 5. (a) Plot of the force measured at the modulation frequency of the test-mass charge against the applied compensation voltage on the x electrodes. (b) The measured force at ω_{mod} plotted as a function of test-mass displacement along x .

To make an in-band measurement of the stray voltages in the sensor we measure the coupling of an oscillating test-mass charge with the torque on the pendulum. This is achieved by applying a slowly varying in-phase voltage to the y -axis sensing electrodes which produce a modified test-mass potential of $V_{\text{TM}} + \alpha_y V_{\text{mod}} \sin(\omega_{\text{mod}} t)$ ($\alpha_y = \sum C_y / C_T$). From (3), it can be shown that the resulting force on the test mass contains a signal at the modulation frequency which has a component proportional to the test-mass displacement and another to the DC voltage imbalance around the x -axis sensor surfaces. The force at twice the modulation-voltage frequency is also proportional to the test-mass displacement. By moving the sensor to null this term, the signal at the measurement frequency is only dependent on the stray DC voltages. This signal can itself be nulled by applying a suitable combination of voltages to the x sensing electrodes. We define the total stray voltage around x , as the sum of the voltages applied to null this signal.

Figure 5(a) shows the magnitude of the measured force signal against the applied compensation voltage. The compensation voltage required to null force signal was found to be -120 mV. Also shown, in figure 5(b), is the magnitude of the component of the force at $2\omega_{\text{mod}}$, a test-mass displacement, $x_0 = 7 \mu\text{m}$ was sufficient to null this signal. Although this measurement is sensitive to different combinations of stray voltages on the sensor x surfaces from those made with the 1-mass pendulum, the magnitude of the effect is consistent with previous measurements [9].

5. Stiffness

In general, any force on the test mass can be expanded to first order about the centre of the sensor as a term independent of position plus the force gradient, or ‘stiffness’ multiplied by the test-mass displacement.

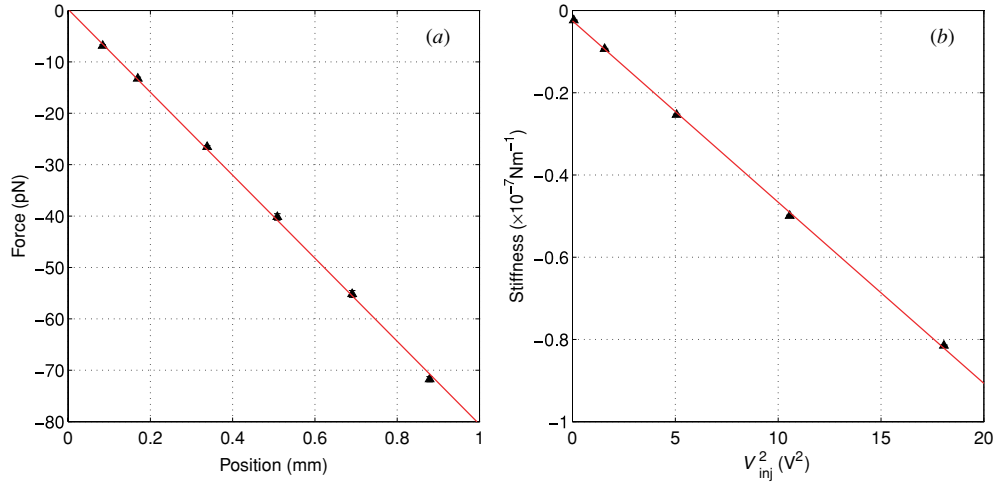


Figure 6. (a) A plot of the position-dependent force on the test mass. (b) The dependence of stiffness on injection voltage, the intercept is the remnant stiffness from all sources other than the AC injection voltages. Errorbars are smaller than the data markers.

The 100 kHz injection voltages are an important source of stiffness in the sensor. The force in V_{TM}^2 from (3) produces a $\sin^2(\omega_{\text{inj}} t)$ term which produces a stiffness due to the injection voltage of

$$\frac{\partial F_x}{\partial x} = -\alpha^2 V_{\text{inj}}^2 \sum_i \frac{\partial^2 C_i}{\partial x^2}. \quad (5)$$

Other sources of stiffness arise from the charge of the test mass and stray voltages on the sensor electrodes, however, since these are kept small by design we expect the contribution from the injection voltages to dominate.

The position-dependent forces on the test mass coming from the sensor can be measured by simply moving the sensor back and forth with a given frequency and with a displacement of up to a millimetre. The position of the test mass in the sensor can be derived from a combination of the autocollimator and capacitive readout. The ratio between the measured force at the frequency at which the motor is moved to the distance the test mass moves is then the total stiffness. This measurement was carried out for various step-sizes, if the first order expansion is valid, the force on the test mass at the measurement frequency should be in proportion to the displacement. We repeated the measurement of the stiffness for several values of V_{inj} to explore the prediction of (5). The residual stiffness at $V_{\text{inj}} = 0$ is the total coming from all other sources.

The position dependence of forces on the test mass is shown in figure 6(a). The position dependence is linear over the range of measurement for test-mass displacements in the sensor of up to 800 μm . Plotting the measured stiffness as a function of the AC injection bias voltage squared, shown in figure 6(b), we find a straight line as predicted by (5). The slope of the fit— $-4.41 \pm 0.01 \times 10^{-9} \text{ N m}^{-1} \text{ V}^{-2}$ —agrees well with the value of $-4 \times 10^{-9} \text{ N m}^{-1} \text{ V}^{-2}$, as predicted by a simple parallel plate model of the electrode capacitances of the GRS.

While the stiffness due to injection voltages is important, it is well modelled and understood; measuring the unmodelled stiffness produced by the sensor is also critical. The intercept of figure 6(b) gives the total remnant stiffness from all sources other than the injection

voltage, $-2.5 \pm 0.1 \times 10^{-9} \text{ N m}^{-1}$. Since during this measurement the test-mass charge was reduced to near zero the most likely contributor is the uncompensated stray DC bias voltages on the x electrodes. A stray voltage level of $\sim 100 \text{ mV}$ as measured in the preceding section would be consistent with the remnant stiffness measured here. This remnant level of stiffness is negligible compared to the total *LISA Pathfinder* budget of $27 \times 10^{-7} \text{ N m}^{-1}$ and even the more stringent *LISA* requirement of $6 \times 10^{-7} \text{ N m}^{-1}$ [13].

6. Conclusions and testing the flight-model replica

As well as making the first measurements sensitive to all on-axis forces arising from a *LISA*-like gravitational reference sensor, the testing campaign described here has also demonstrated the suitability of the 4-test-mass pendulum for the task of testing the *LISA Pathfinder* flight-model replica GRS. This sensor is an exact replica of the instrument that will be launched on the spacecraft save for a relaxation of some machining and assembly requirements. This testing is therefore vital for ensuring there are no aspects of the sensor design that will jeopardize the goals of the *LISA Pathfinder* mission. In addition to the sensor, we will test a replica of the flight-model front-end electronics which is crucial to the performance of the GRS.

The tests performed and reported here make up the core of the test campaign using the flight-model replica, in addition there will be measurements of the noise coming from the front-end electronics, as well as demonstration of the capacitive force and torque actuation and the UV-light discharge system for neutralizing the test mass.

The findings of these tests confirm previous measurements made with the 1-test-mass torsion pendulum using the same sensor. Although the measured force sensitivity of the 4-test-mass pendulum is not yet at its thermal limit, it has proved itself able to make measurements highly representative of those to be carried out in-flight on *LISA Pathfinder*. The effect of all forces along the x -axis of the test-mass are measurable and depend only on a trivial rule for converting torque to force. Specific disturbances can be measured exactly as they will occur in-flight, in the case of thermal-gradient effects and stiffness measurement, a force measurement is significantly simpler than measuring a torque. The result is that these effects can be measured easily with very high precision. Recent upgrades to the 1-mass facility [14] may mean that this pendulum could be well suited to supplementary measurements of the force noise and stray DC voltage stability using the flight-model replica.

Acknowledgments

The authors would like to thank the INFN and ASI for support of this work.

References

- [1] Bender P L *et al* 1998 Laser interferometer space antenna for the detection and observation of gravitational waves *Pre-phase A report* 2nd edn
- [2] Anza S *et al* 2005 The LTP experiment on the *LISA Pathfinder* mission *Class. Quantum Grav.* **22** 125
- [3] Dolesi R *et al* 2003 Gravitational sensor for *LISA* and its technology demonstration mission *Class. Quantum Grav.* **20** 99
- [4] Hueller M, Cavalleri A, Dolesi R, Vitale S and Weber W J 2002 Torsion pendulum facility for ground testing of gravitational sensors for *LISA* *Class. Quantum Grav.* **19** 1757–65
- [5] Carbone L *et al* 2005 Characterization of disturbance sources for *LISA*: torsion pendulum results *Class. Quantum Grav.* **22** 509
- [6] Carbone L *et al* 2003 Achieving geodetic motion for *LISA* test masses: ground testing results *Phys. Rev. Lett.* **91** 151101

- [7] Carbone L *et al* 2007 Upper limits to surface-force disturbances on LISA proof masses and the possibility of observing galactic binaries *Phys. Rev. D* **75** 042001
- [8] Carbone L *et al* 2007 Thermal gradient-induced forces on geodesic reference masses for LISA *Phys. Rev. D* **76** 102003
- [9] Weber W J *et al* 2007 Possibilities for measurement and compensation of stray DC electric fields acting on drag-free test masses *Adv. Space Res.* **39** 213–8
- [10] Wass P J *et al* 2006 Testing of the UV discharge system for LISA Pathfinder *Laser Interferometer Space Antenna: 6th Int. LISA Symp. (American Institute of Physics Conference Series vol 873)* ed S M Merkowitz and J C Livas pp 220–4
- [11] Ciani G 2008 Free-fall of LISA test masses: a new torsion pendulum to test translational acceleration (Dipartimento di Fisica, Università di Trento)
- [12] Carbone L *et al* 2006 Torsion pendulum facility for direct force measurements of LISA GRS related disturbances *Laser Interferometer Space Antenna: 6th Int. LISA Symp. (American Institute of Physics Conference Series vol 873)* ed S M Merkowitz and J C Livas pp 561–565
- [13] Vitale S *et al* 2005 Science requirements and top-level architecture definition for the LTP on board LISA Pathfinder. LISA Pathfinder Science requirements document LTPA-UTN-ScRD Issue 3
- [14] Cavalleri A *et al* 2009 A new torsion pendulum for testing the limits of free-fall for LISA test masses *Class. Quantum Grav.* **26** 094017